ISSN 0869-5911, Petrology, 2023, Vol. 31, No. 5, pp. 475–491. © Pleiades Publishing, Ltd., 2023.
Russian Text © The Author(s), 2023, published in Petrologiya, 2023, Vol. 31, No. 5, pp. 463–481.

Variations in the Composition of MORB Chilled Glasses from the Mid-Atlantic Ridge, 12°–31° N: Reflection of Compositional Evolution of Parental Melts and the Influence of a Hydrothermal Component

S. A. Silantyev[a], *, A. I. Buikin[a], A. R. Tshovrebova[a], V. V. Shabykova[a], and V. E. Bel'tenev[b]

[a] *Vernadsky Institute of Russian Academy of Sciences, Moscow, 119991 Russia*

[b] *VNIIOkeangeologia, St-Petersburg, 190121 Russia*

**e-mail: silantyev@geokhi.ru*

Received September 29, 2022; revised December 2, 2022; accepted January 15, 2023

Abstract—The geochemical peculiarities of sample collection of MORB chilled glasses obtained in six areas of the axial zone of the Mid-Atlantic Ridge (MAR), 12°–31° N have been studied. The results of this study provided information on the composition of the parental melts for these glasses and made it possible to assess the probable geochemical effects reflecting the interaction of magmatic melts with hydrothermal systems of the MAR axial zone or with altered oceanic crust (AOC). It is shown that basalts of the E-MORB family which includes most samples are localized mainly in the "cold" segments of the MAR, in the crustal section dominated by serpentinites. On the other hand, samples with depleted signatures (N-MORB) belong to MAR segments where serpentinite outcrops either are absent or play a subordinate role. The E-MORB chilled glasses from "cold" segments of the MAR show signs of contamination of basaltic melts with components assimilated either from the host serpentinites or from aqueous–saline fluids circulating in hydrothermal systems located in serpentinites ("serpentinite hosted"). Judging by the data obtained on the nature of Cl, U, and Sr variations in the studied chilled glasses ascribed to the N-MORB family, there are no signs of intracrustal contamination. It is assumed that relics of the ancient continental lithosphere preserved under axial zone of the MAR and involved in the partial melting of the shallow mantle took part in the formation of E-MORB parental melts in some MAR segments.

Keywords: Mid-Atlantic Ridge, MORB, partial melting, hydrothermal systems, non-spreading block

DOI: 10.1134/S0869591123050053

INTRODUCTION

One of the fundamental phenomena that determine the structure and composition of oceanic crust of the Mid-Atlantic Ridge (MAR) is its geochemical along-strike segmentation expressed in the alternation of segments made up of depleted basalts (N-MORB) and their enriched varieties (E-MORB). The geochemical segmentation, the signs of which were found in the magmatic products of the MAR rift valley, is discussed in many works (Schilling et al., 1983; Klein and Langmuir, 1987; Bougault et al., 1988; Bonatti et al., 1992; Dmitriev, 1998; Dosso et al., 1999). The main factors responsible for the observed heterogeneity in the distribution of indicator geochemical parameters of MORB along MAR axis are the compositional heterogeneity of mantle protolith beneath the rift valley and different degrees of its melting. Geochemical variations of basalts along MAR axis indicate also a mixture of parental E- and N-MORB melts, which determine the peculiarities of the volcanic products in transitional zones between anomalous and normal MAR segments (e.g., Eason and Sinton, 2006). Another characteristic feature of the MAR axial zone consists in the wide distribution of signs of hydrothermal activity, which facilitates the formation of large hydrothermal occurrences. The discovery of the Semenov hydrothermal field located between the known Ashadze (12°58′ N) and Logatchev (14°45′ N) fields made it possible to regard the clusters of hydrothermal fields as a common element of MAR basement in the Central Atlantic. Based on character of observed correlations between rheological and petrological-geochemical segmentation of MAR (Sokolov et al., 2020), two contrasting spreading regimes in the axial zone of this ridge are driven by two geodynamic scenarios: (1) formation of normal Penrose-type basaltic crust in "hot" segments of MAR; (2) formation of the Hess-type oceanic crust in MAR cold segments, which consists mainly of residual mantle peridotites and gabbroids, at reduced or absent basaltic

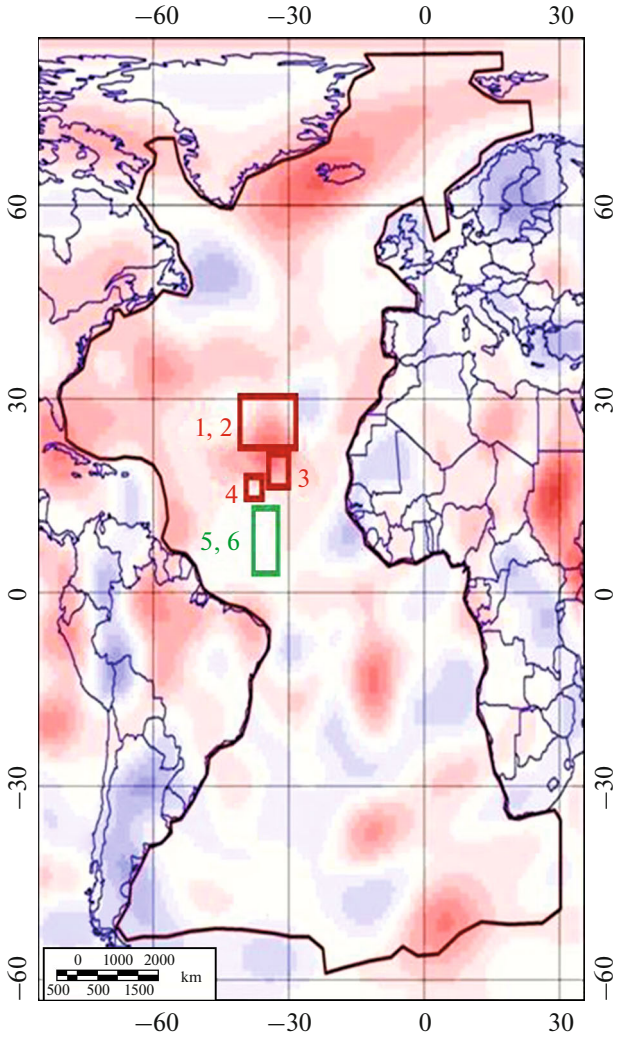

Fig. 1. Horizontal section of volume variations of the S-wave velocities along MAR axis strike at a depth of 300 km calculated in (Dmitriev and Sokolov, 2003) according to data of digital seismic tomography model TX2011 (Grand, 2002) taken from https://ds.iris.edu/spud/earthmodel/10131216. The red color shows the negative anomalies related to the decrease of seismic wave velocities in "hot" segments, while blue color shows the positive anomalies of "cold" segments. Red boxes show the areas of the MAR axial zone with the wide distribution of basaltic rocks, where samples of chilled glasses corresponding to groups 1–4 in Table 1 were obtained. Green boxes outline the MAR areas, in which oceanic basement is mainly made up of peridotites and where chilled glasses of groups 5–6 were obtained.

magmatism. Empirical data on the structure of crust in the axial MAR zone are well consistent with seismic tomography data, which makes it possible to reconstruct the distribution of rheological mantle heterogeneities. It is generally accepted that the S-wave (shear wave) variations reflect the thermal state of mantle (e.g., Grand et al., 1997; Becker and Boschi, 2002). The distribution pattern of $d(V_p/V_s)$ in a mantle layer beneath MAR corresponding to a depth of 300 km is shown in Fig. 1. Obviously, the normal ridge segments made up of basaltic rocks are alternated with anomalous (relative to canonical spreading model) segments composed of ultramafic rocks along the strike of the MAR axial zone in the northern hemisphere. In compliance with this tendency, the hydrothermal fields and occurrences of MAR form two families: Broken Spur, Snake Pit, TAG, Lucky Strike, Surprise, Yubileinoe, Zenith-Victoria, and Krasnov fields enclosed in the basaltic protolih; and serpentinite-hosted Ashadze, Semenov, Logatchev, Lost City, and Rainbow fields. This indicates an unambiguous relationship between hydrothermal activity in MAR and its compositional segmentation (Bogdanov et al., 2006; Silantyev et al., 2009; Andreani et al, 2014; Firstova et al., 2016). The distribution of two indicated types of hydrothermal fields along MAR axis resulted in the conclusion that the hydrothermal systems related to the basaltic protolith are formed in a setting of cooling lithosphere, whereas serpentinite-hosted hydrothermal systems are produced at heating of cold lithosphere. This suggests a relationship between geochemical peculiarity of hydrothermal processes in the MAR axial zone and its compositional segmentation. The geochemical peculiarity of hydrothermal systems of MOR depends on the type of host crustal section. The effect of host rocks on the composition of hydrothermal edifices of rift valley is demonstrated by the differences in the content of some elements in the serpentinite- and basalt-hosted massive sulfide ores from black smoker tubes of MAR (e.g., Firstova et al., 2016).

The aim of this study was to estimate the possible influence of active hydrothermal systems on the geochemical parameters of MORB, which serve as traditional indicators of genetic conditions and geochemical nature of mantle sources of magmatism in oceanic spreading centers. This work is a continuation of studies launched in work (Buikin et al., 2022), where analysis of noble gases and nitrogen isotopic composition and H_2O and Cl contents in samples of chilled glasses of the MAR rift valley at 16°07′–17°11′ N led the authors to suggest that the signs of contamination by non-mantle noble gases and nitrogen observed in these glasses serve as evidence for the interaction of magmatic melt with a high-temperature hydrothermal fluid. For this reason, samples for our study were chosen based on the following criteria: the absence of petrographic features of postmagmatic alterations; weight sufficient to determine the isotopic compositions of noble gases, nitrogen, and CO_2 (5–7 g of pure glass); the wide compositional range describing the whole diversity of geochemical types of MORB. These criteria strongly constrained the choice of samples. In spite of this, available sample collection completely corresponds to the indicated requirements and includes samples of chilled glasses obtained in the rift valley areas that contain hydrothermal fields hosted in two major types of oceanic crust: one type related to

basalts, and other, to serpentinites. Thus, geochemical data on the studied chilled glasses provide insight not only in the composition of parental melts, but also into possible geochemical effects reflecting the interaction of parental melts with hydrothermal solutions.

METHODS

The contents of major elements in chilled glasses from the studied collection were determined at the GEOKHI RAS (Moscow) using SX 100 (CAMECA) microprobe with four vertical spectrometers at an accelerating voltage of 15 kV and beam current of 30 nA (analyst N.N. Kononkova). The composition of glasses and olivine and plagioclase crystallites in them was estimated using a TESCAN MIRA3 FEG SEM (Field Emission Gun—Scanning Electron Microscope) equipped with an ULTIM MAX 100 energy dispersive spectrometer (Oxford Instruments) using Aztec 5.0 software (GEOKHI RAS). The quantitative analysis was carried out at an accelerating voltage of 20 kV and beam current of 1.4 nA, collecting 10^6 pulses for each measurement. Pure elements and compounds were used as standards. The measurement accuracy of major elements was 2 rel %, and the threshold of calculated content of trace elements was 3σ.

The REE and trace element contents in samples of chilled glasses were determined by secondary ion mass spectrometry (SIMS, ion probe) at the Yaroslavl Branch of the Valiev Institute of Physics and Technology of the Russian Academy of Sciences (YaF FTIAN RAS) using CAMECA IMS-4F secondary ion microscope. Samples for analyses were prepared as thin sections coated by gold layer 0.03 μm thick with magnetron sprayer. The technique was described in (Smirnov et al., 1995; Nosova et al., 2002; Fedotova et al., 2008).

The primary beam of O_2^- ions was accelerated to 10 keV and focused to a ~ 20–30 μm spot. The intensity of primary ion current was 5 nA (protocol "volatiles") and 2 nA (main protocol). Thereby, secondary ions were collected from an area limited by a field aperture of 10 and 25 μm, respectively, which together with beam focusing constrained the analyzed spot size. The secondary ions were collected with an energy bandpass of 75–125 eV using an energy offset of –100 V from 4500 V acceleration with an energy window of 50 eV. A change of potential of analyzed area due to sample charging under the ion bombardment was corrected using a special procedure of automated adjustment of sample potential. The mass spectral resolution was $M/\Delta M = 500$.

Analyzed area was sputtered for two–three minutes with a beam rastered across a 30 × 30 μm area to remove the conductive film and surface contamination from an area of 50 × 50 μm. Each measurement involved five counting cycles with a discrete transition between mass peaks within the given set of elements. The counting time varied depending on the signal intensity and was determined automatically by statistical control. The maximum counting time for each component was no more than 30 s in each cycle.

Absolute concentrations for each element were calculated based on the measured intensities of positively charged secondary ions normalized to the intensity of secondary ions $^{30}Si^+$, using coefficients of relative sensitivity (CRS): $C_i = I_i/I^{30}Si \times K_i$. Calibration dependences were obtained experimentally using sets (7–13) of known well-certified standard samples (Jochum et al., 2000).

Signals of $^{153}Eu^+$, $^{174}Yb^+$, $^{158}Gd^+$, and $^{167}Er^+$ were purified from molecular ion interference of Ba oxides and lighter REE using subtraction schemes proposed in (Bottazzi et al., 1994). A contribution of $^{143}Nd^{16}O^+$ was taken into account during determination of $^{159}Tb^+$. The NdO interference contributed in determining Yb and Gd. For $^{165}Ho^+$ correction, the intensity of $^{149}Sm^{16}O^+$ was calculated by multiplying the measured $^{149}Sm^+$ intensity on the corresponding coefficient. The ratio of $^{149}Sm^{16}O^+/^{149}Sm^+ = 0.2$ was found experimentally using a set of standard samples (Jochum et al., 2000) based on the measurement of intensities of $^{149}Sm^+$ and mass peaks within 166–170 a.m.u., which correspond to the erbium and samarium isotopes.

The measurement error of trace elements is conditionally characterized by 5–15% for concentrations >1μg/g and 15–30% for concentrations of 1–0.1 μg/g.

GEOLOGICAL OUTLINE OF SAMPLING AREAS OF THE MAR AXIAL ZONE

The studied samples of chilled glasses were collected in six areas of the MAR axial zone, which are arranged along its strike between 12° and 31° N (Table 1, Fig. 1). According to (Hemond et al., 2006; Sokolov et al., 2020), these areas are characterized by different structure of oceanic crust section and based on the predominant rock types are subdivided into two major groups. One group includes the MAR segments dominated by basalts (30°–31° N, 26° N, and 16°–18° N). The other group includes segments made up mainly of serpentinite exposures with subordinate gabbroid bodies (20°–21° N, 14°–15° N, and 12°–14° N).

The rift valley area limited by 30°–31° N is located to the south of the Petrov Fracture Zone. Chilled glasses obtained here were dredged on an axial rise within the rift valley. Judging from data reported in (Klitgord et al., 1993), the rift valley floor in this area is made up of fresh pillow basalts with unaltered chilled glasses, which, according to their position, are ascribed to the youngest manifestations of the basaltic magmatism of rift valley (so called "zero age MORB"). The Broken Spur hydrothermal field located to the south of chilled glass sampling locality is related to active volcanic center on the axial rise of the MAR rift valley at 29°10′ N (Murton et al., 1995).

Table 1. Sampling localities of studied chilled glasses and their geological position

Sample no.	Research vessel and cruise no.	Sampling locality	Nearest hydrothermal field	Northern latitude	Western longitude	Depth, m
16ABP7-8	*Akademik Boris Petrov*, 16	AURV	Broken Spur (29)	30.58	41.88	3470–3319
64gl	*Professor Logachev,* 6	RV	TAG (26)	26.06	44.85	*
14-3/1gl	*Professor Logachev*, 6	RV	TAG (26)	26.14	44.81	*
36L12D-3	*Professor Logachev*, 36	EWRV	Surprise (20.75)	20.76	45.64	2915–2826
36L29D-4	*Professor Logachev*, 36	EWRV	Surprise (20.75)	20.59	45.79	3153–3041
36L40D-3	*Professor Logachev*, 36	WWRV	Zenith-Victoria (20.13)	20.14	45.75	2458–2337
36L44D-3	*Professor Logachev*, 36	WWRV	Zenith-Victoria (20.13)	20.14	45.73	2970–2706
36L46D-2	*Professor Logachev*, 36	EWRV	Yubileinoe (20.15)	20.15	45.62	2739–2510
36L233D-1	*Professor Logachev*, 36	EWRV		17.90	46.58	3350–3000
36L235D-1	*Professor Logachev*, 36	EWRV		17.94	46.61	3201–3180
16ABP54gl	*Akademik Boris Petrov*, 16	WWRV		15.42	46.68	4186–3700
16ABP65-34	*Akademik Boris Petrov*, 16	WWRV		15.04	44.95	3699–3518
16ABP67-7	*Akademik Boris Petrov*, 16	WWRV	Logatchev (14.75)	14.86	45.03	3813–3562
16ABP67-9	*Akademik Boris Petrov*, 16	WWRV	Logatchev (14.75)	14.86	45.03	3813–3562
16ABP69-10	*Akademik Boris Petrov*, 16	WWRV	Logatchev (14.75)	14.76	45.10	3500–3225
16ABP69-11	*Akademik Boris Petrov*, 16	WWRV	Logatchev (14.75)	14.76	45.10	3500–3225
16ABP69-13	*Akademik Boris Petrov*, 16	WWRV	Logatchev (14.75)	14.76	45.10	3500–3225
16ABP70-31	*Akademik Boris Petrov*, 16	WWRV**		15.08	44.98	2500–2450
16ABP70-32	*Akademik Boris Petrov*, 16	WWRV**		15.08	44.98	2500–2450
16ABP70-34	*Akademik Boris Petrov*, 16	WWRV**		15.08	44.98	2500–2450
16ABP71-13	*Akademik Boris Petrov*, 16	WWRV**		15.08	44.95	3068–2629
2PD44-1	*Akademik Boris Petrov*, 2	WWRV	Logatchev (14.75)	14.33	45.05	3295
2PD44-3	*Akademik Boris Petrov*, 2	WWRV	Logatchev (14.75)	14.33	45.05	3295
2PD45	*Akademik Boris Petrov*, 2	AURV	Logatchev (14.75)	14.50	44.83	3850
2PD43-3	*Akademik Boris Petrov*, 2	AURV	Semenov (13.50)	13.77	45.03	3510

(RV) rift valley, (EWRV) eastern wall of the rift valley, (WWRV) western wall of the rift valley, (AURV) axial uplift in the rift valley, (NFZ) non-transform fracture zone.
* Data are absent; ** samples were collected on inner corner uplift located at the intersection of the rift valley with 15°20′ Fracture Zone. Coordinates (northern latitude) are shown beneath name of the corresponding hydrothermal field. All coordinates are given on a decimal scale.

The well-studied TAG hydrothermal field is located in the segment of the MAR axial zone at 26° N, being confined to the rift valley eastern wall, which is made up of basalts and characterized by the sharp morphological asymmetry and highly rugged topography (Rona et al., 1993). Data reported in (Rona et al., 1980; Humphris et al., 2015) indicate the widespread signs of hydrothermal transformation of basaltic protolith expressed in the TAG hydrothermal field area: basaltic rocks developed here contain mineral assemblages of greenschist and zeolite facies.

In the MAR segments between 20° and 21°, the crust section consists both of basalts and ultramafic rocks and gabbroids (Casey, 1997; Dick et al., 2010). Silantyev et al. (2015) suggest the presence of shallow magma chambers beneath the MAR axial zone in this area, which serve as the main heat source for the initiation of active hydrothermal system. During Cruise of R/V Professor Logachev, the hydrothermal fields Surprise (20°45.4′ N), Yubileinoe (20°09′ N), and Zenith-Victoria (20°08′ N) were discovered in the walls of the rift valley in this segment of the MAR axial zone. The Surprise field is located in the eastern wall of the rift valley, on the slope of volcanic uplift (Beltenev et al., 2017). The rift zone wall, where the Yubileinoe field is exposed, contains large blocks made up of basalts (Sukhanova, 2018). The area of the Zenith–Victoria hydrothermal field reveals signs of high tectonic activity, which are expressed in the peculiar submarine topography (Sukhanova, 2018). This hydrothermal field is located within the volcanic uplift in the rift valley (Cherkashov et al., 2010).

The axial MAR zone between 16° and 18° N has been poorly studied. In this segment, it is sharply dominated by basalts; to the north of this area, between 19° and 20° N, basalts and peridotites occur in almost equal proportions (Silantyev et al., 2015). To the south of sampling site of chilled glasses, the large Pobeda hydrothermal cluster was found and sampled during Cruise 37 of the R/V *Professor Logachev* in the eastern wall of the rift valley made up of plutonic rocks forming core complex (Beltenev et al., 2016; Maslennikov et al., 2020). However, samples uplifted from dredging site indicate the abundance of fresh pillow basalts with abundant crusts of chilled glasses. Inactive Krasnov hydrothermal field is located to the south of the Pobeda ore cluster at 16°38′ N. This occurrence is the largest known ore field of MAR, being confined to the highly deformed block of oceanic crust consisting of brecciated basalts. The Krasnov field is located to the east of the axial rise in the crest part of the eastern wall of rift valley (Bel'tenev et al., 2004).

The area of the MAR axial zone enclosed within 14°–15° N is one of the best studied areas of Central Atlantic, which includes the 15°20′ Fracture Zone (Cape Verde) displacing the rift valley by almost 200 km. The thalweg of the fracture and MAR segments adjoining from the south and north contain widespread serpentinites and their breccias. In this area, basaltic magmatism is extremely scarce, which indicates disagreement between thickness of basaltic layer estimated by geochemical methods and true structure of oceanic crust, which is characterized in this area by the sharp predominance of serpentinites (e.g., Cannat and Casey, 1995). Deepsea drilling (*Shipboard ...*, 2003) and numerous dredging (Silantyev, 2003) showed that abyssal peridotites are abundant in both walls of the rift valley of MAR segments, which adjoin the fracture zone from the south and north. The sharp-gradient geochemical anomaly located in the MAR axial zone within 14°–15° N is expressed in the presence of products of basaltic magmatism, which are strongly enriched in the incompatible elements and ascribed to typical E-MORB (Bougault et al., 1988; Dosso et al., 1991). The large Logatchev hydrothermal field is located in the considered water basin, at 14°45′ N, being confined to the marginal scarp of the rift valley eastern wall made up of serpentinites.

The Ashadze hydrothermal field (12°59′ N), which is located 200 km south of the Logatchev hydrothermal field, together with the Semenov hydrothermal field situated slightly northward (13°30′ N) and Logatchev field, forms the largest hydrothermal cluster of MAR. The Ashadze hydrothermal field is located in the rift valley western wall where basalts occur in subordinate amounts, while serpentinites and gabbros are predominant rocks (*Shipboard ...*, 2007). The Semenov hydrothermal field, as the Ashadze hydrothermal field, is located in the western wall consisting of rock associations of core complexes: serpentinites, gabbroids, plagiogranites, and subordinate basalts and dolerites (Melekestseva et al., 2018). In the vicinity of the Semenov hydrothermal field, in the axial rise of the rift valley at 13°46′ N, famous "popping rocks"—strongly porous basalts with abundant gaseous inclusions in chilled matrix—were dredged during Cruise 2 of the R/V *Akademik Boris Petrov* (Sarda and Graham, 1990).

GEOCHEMISTRY OF THE STUDIED CHILLED GLASSES FROM THE MAR AXIAL ZONE

Contents of major elements in the studied chilled glasses are presented in Table 2. According to the generally accepted classification based on the indicator K_2O/TiO_2 ratio, two main families of tholeiitic basalts of the oceanic spreading centers are distinguished: N-MORB (depleted) and E-MORB (enriched) (e.g., Wilson, 1989; Dmitriev, 1998). Basalts transitional between N-MORB and E-MORB are termed as T-MORB (transitional MORB) (e.g., Schilling et al., 1983; Eason and Sinton, 2006). MORB with extremely low $K_2O/TiO_2 \le 0.05$ are ascribed to the most depleted varieties of the mid-ocean ridge basalts– D-MORB (Shimizu et al., 2016). The compositional variations in chilled glasses shown in Fig. 2 demonstrate that the studied samples span the entire

Table 2. Contents of major elements in the studied chilled glasses

Sample no.	SiO_2	TiO_2	Al_2O_3	FeO*	MnO	MgO	CaO	Na_2O	K_2O	Total
16ABP7-8	50.90	1.56	14.47	9.55	0.13	9.27	10.85	2.16	0.55	99.43
64gl	51.23	1.56	15.13	9.63	0.17	8.63	11.44	3.13	0.13	101.04
14-3/1gl	50.79	1.40	15.60	9.45	0.16	9.15	11.77	3.21	0.11	101.62
36 L12D-3	50.21	1.56	15.76	9.77	0.18	8.59	11.76	3.36	0.13	101.32
36 L16D-3	50.28	1.20	15.34	9.31	0.16	9.77	12.27	2.56	0.09	100.98
36 L29D-4	51.03	1.51	15.11	9.30	0.15	9.10	11.72	3.12	0.14	101.17
36 L40D-3	50.89	1.43	14.99	9.63	0.16	8.32	12.42	3.01	0.11	100.96
36 L44D-3	50.62	1.69	15.21	9.75	0.18	7.99	11.84	3.40	0.11	100.80
36 L46D-2	50.58	1.58	15.17	9.71	0.17	8.21	12.09	3.20	0.10	100.81
36 L233D-1	50.26	1.50	15.07	10.06	0.21	9.18	11.47	3.04	0.19	100.98
36 L235D-1	50.76	2.08	14.04	11.73	0.17	8.18	10.97	3.24	0.13	101.31
16ABP54 gl	52.05	1.72	14.51	10.19	0.23	7.39	11.03	3.38	0.28	100.79
16ABP70-31	52.09	1.60	15.01	9.03	0.19	7.80	11.45	3.00	0.48	100.65
16ABP71-13	51.10	1.09	15.13	9.38	0.10	9.30	12.31	2.48	0.20	101.09
16ABP67-9	51.95	1.59	14.48	9.09	0.15	8.99	11.17	2.47	0.54	100.42
16ABP70-32	51.35	1.51	15.04	9.39	0.17	7.24	11.30	2.93	0.46	99.39
16ABP65-34	51.15	1.32	14.98	9.18	0.19	8.71	11.52	2.68	0.42	100.16
16ABP69-13	50.87	1.11	15.29	9.32	0.17	8.97	12.43	2.51	0.22	100.88
16ABP69-11	50.57	1.09	15.11	9.34	0.21	9.27	12.27	2.51	0.23	100.59
16ABP 69-10	50.05	1.01	15.30	9.56	0.20	9.02	12.36	2.19	0.21	99.91
16ABP70-34	50.93	1.49	14.93	9.17	0.22	7.79	11.32	2.93	0.49	99.28
16ABP 67-7	51.43	1.27	14.87	9.60	0.18	7.86	11.90	2.73	0.32	100.16
2PD44-1	50.16	1.59	15.32	11.00	0.23	6.92	11.18	3.03	0.55	99.98
2PD44-3	51.01	1.90	14.48	10.62	0.13	6.54	10.81	3.17	0.59	99.25
2PD45	51.11	1.65	14.57	9.85	0.19	7.57	10.97	2.99	0.53	99.43
2PD40-2	49.89	1.79	14.75	10.62	0.12	8.53	11.77	2.94	0.05	100.47
2PD43-3	50.65	1.60	14.80	9.85	0.14	8.08	10.92	3.26	0.26	99.55

Composition of each sample is given as average of three individual glass segments. All iron as FeO. Contents of oxides are given in wt %.

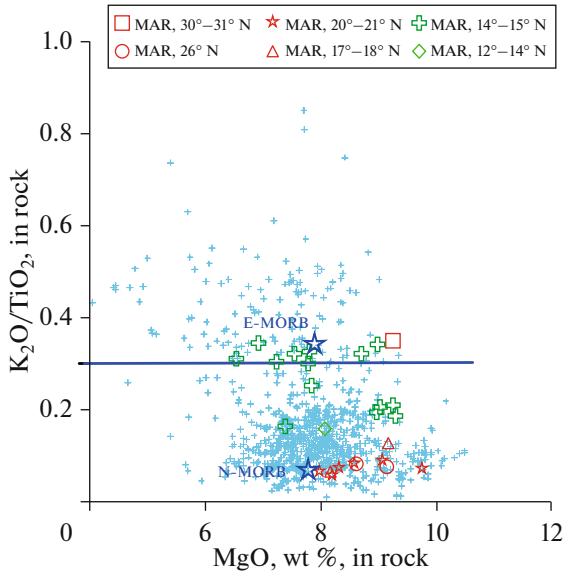

Fig. 2. Variations of MgO and K_2O/TiO_2 in the studied chilled glasses (determined on microprobe). Blue crosses correspond to compositions taken from (RIDGE ..., 1999). Red symbols designate data points of the studied chilled glasses dredged in the rift valley areas made up mainly on basalts. Green symbols show the compositions of chilled glasses from the MAR axial zone areas consisting mainly of serpentinites. The compositions of N-MORB and E-MORB marked by large blue asterisks are given according to (Wilson, 1989).

spectrum of the geochemical MORB types and include chilled glasses formed at different degrees of fractionation of tholeiitic melts. Discriminant line between N-MORB and E-MORB fields was drawn using data from (Wilson, 1989; Dmitriev et al., 2006).

REE data presented in Table 3 indicate that chilled samples collected in the MAR rift zone between 12° and 31° N are ascribed to two main groups, one of which include chilled glasses with $(La/Sm)_{cn} \le 1$, whereas the other group, samples with $(La/Sm)_{cn} \ge 1$. As follows from Figs. 3 and 4, practically all samples of chilled glasses showing LREE enrichment were obtained in MAR segments enclosed between 12° and 15° N. The exception is sample 16ABP7-8, which, as mentioned above, was dredged in the axial uplift within the rift valley. Data points of chilled glasses with $(La/Sm)_{cn} \ge 1$, falling in the K_2O/TiO_2 range of 0.2–0.3, are shown in Fig. 4 as T-MORB basalts, which could be formed through fractionation and mixing of parental melts. Samples with $(La/Sm)_{cn} \ge 1$ and $K_2O/TiO_2 \ge 0.3$ define a compact group (Fig. 4) corresponding to typical E-MORB. All chilled glasses obtained from segments between 15° and 31° N reveal $(La/Sm)_{cn} \le 1$ and demonstrate the chondrite-normalized REE distribution pattern typical of N-MORB (Fig. 4).

Table 3. Content of rare-earth elements in the studied chilled glasses

Sample no.	La	Ce	Pr	Nd	Sm	Eu	Gd	Tb	Dy	Ho	Er	Yb	Lu
16ABP7-8	13.09	28.93	3.67	17.84	4.10	1.50	4.52	0.63	4.87	0.86	3.36	3.07	0.47
64gl	4.30	13.67	2.14	13.15	4.42	1.47	5.56	0.94	6.98	1.40	4.98	4.92	0.68
14-3/1gl	3.12	9.71	1.66	9.83	3.44	1.24	4.92	0.73	5.49	1.03	3.77	3.80	0.57
36L233D-1	4.93	13.54	2.03	11.77	4.28	1.35	4.06	0.85	5.90	1.21	4.42	4.64	0.64
36L235D-1	4.64	14.99	2.59	16.39	5.67	1.87	6.86	1.09	8.29	1.71	6.11	6.33	0.86
36L12D-3	3.72	11.09	1.90	10.82	3.77	1.38	5.12	0.71	5.75	1.06	3.95	3.75	0.60
36L16D-3	2.64	8.10	1.41	8.95	3.02	1.14	4.46	0.63	5.40	1.13	4.03	4.07	0.59
36L29D-4	3.82	11.21	1.88	11.35	3.76	1.38	4.11	0.72	5.62	1.08	3.76	3.93	0.57
36L40D-3	3.13	9.33	1.68	9.95	3.42	1.33	4.47	0.69	5.77	1.08	3.79	3.83	0.61
36L44D-3	3.86	13.39	2.18	12.98	4.73	1.63	6.92	1.03	6.80	1.33	4.54	4.59	0.69
36L46D-2	3.29	11.82	1.99	12.28	4.21	1.45	4.94	0.84	5.95	1.09	4.02	3.72	0.62
16ABP54gl	8.17	18.98	2.94	15.83	4.34	1.66	5.02	0.89	6.43	1.20	4.77	4.60	0.71
16ABP70-31	12.11	26.30	3.45	15.98	4.28	1.42	4.54	0.58	4.44	0.83	2.91	2.75	0.45
16ABP71-13	5.68	13.91	1.80	9.69	2.49	0.94	3.31	0.44	3.68	0.71	2.59	2.30	0.40
16ABP67-9	13.13	27.15	3.50	16.91	4.21	1.47	4.22	0.60	4.61	0.82	2.67	2.95	0.43
16ABP70-32	12.64	29.11	3.66	16.87	4.74	1.68	5.28	0.76	4.97	0.93	3.60	3.40	0.52
16ABP65-34	10.94	21.86	2.88	13.56	3.66	1.30	3.48	0.53	4.24	0.84	2.74	2.76	0.39
16ABP69-13	6.05	13.49	1.78	9.97	2.52	1.02	2.49	0.46	3.65	0.72	2.47	2.53	0.35
16ABP69-11	5.92	14.80	1.94	10.19	3.06	1.10	3.12	0.53	3.63	0.76	2.44	2.60	0.39
16ABP69-10	5.47	13.24	1.81	9.81	2.63	0.96	3.02	0.46	3.57	0.74	2.50	2.26	0.39
16ABP70-34	12.01	26.14	3.23	15.59	4.07	1.25	4.76	0.67	4.50	0.85	2.82	2.68	0.45
16ABP67-7	7.59	18.23	2.28	11.24	3.49	1.18	4.59	0.56	3.97	0.81	3.03	2.71	0.34
2PD44-1	13.45	29.49	3.54	18.31	4.45	1.49	5.24	0.71	4.94	0.93	3.50	3.18	0.49
2PD44-3	14.76	32.54	3.82	19.12	5.04	1.57	5.03	0.79	5.42	1.10	3.74	3.48	0.55
2PD-45	13.02	28.85	3.51	18.46	4.98	1.53	4.65	0.66	5.13	0.85	3.16	3.08	0.46
2PD43-3	7.37	17.78	2.54	14.43	4.34	1.48	5.65	0.82	5.91	1.13	4.14	3.99	0.55

REE content is given in ppm.

The reliable geochemical indicators of the degree of enrichment of tholeiitic basalts are the Th/La and Ce/U ratios (e.g., Halliday et al., 1995; Shimizu et al., 2016). As REE distribution pattern, Th/La and Ce/U variations in the studied samples suggest that all chilled glasses obtained in the basalt-dominated segments are ascribed to N-MORB, resembling the most depleted N-MORB varieties, D-MORB, for sample 36L46D-2 (Table 4, Fig. 5).

The behavior of strontium during formation of the basaltic protolith of oceanic crust is characterized by two major trends: one trend is determined by fractionation crystallization of parental melt (e.g., Winter, 2001); the other trend is related to the low-temperature transformation of basalts, including palagonitization of their chilled glass (e.g., Verma, 1992). Variations of Sr, MgO and K_2O/TiO_2 (Fig. 6) indicate that chilled glasses ascribed to N-MORB show an increase of Sr content without significant changes of K_2O/TiO_2 (Fig. 6a). Such a strontium behavior could be caused by the formation of plagioclase crystallites in chilled glass, as, for instance, was established in sample 14-3/1gl (Fig. 7b). Some samples of chilled glasses with N-MORB characteristics (sample 36L235D-1) contain also olivine crystallites (Fig. 7a). This explains the higher CaO and Al_2O_3 contents in sample with plagioclase crystallites compared to sample with olivine crystallites. Presented data suggest that variation trends of strontium in the studied glasses are mainly related to the fractional crystallization of parental

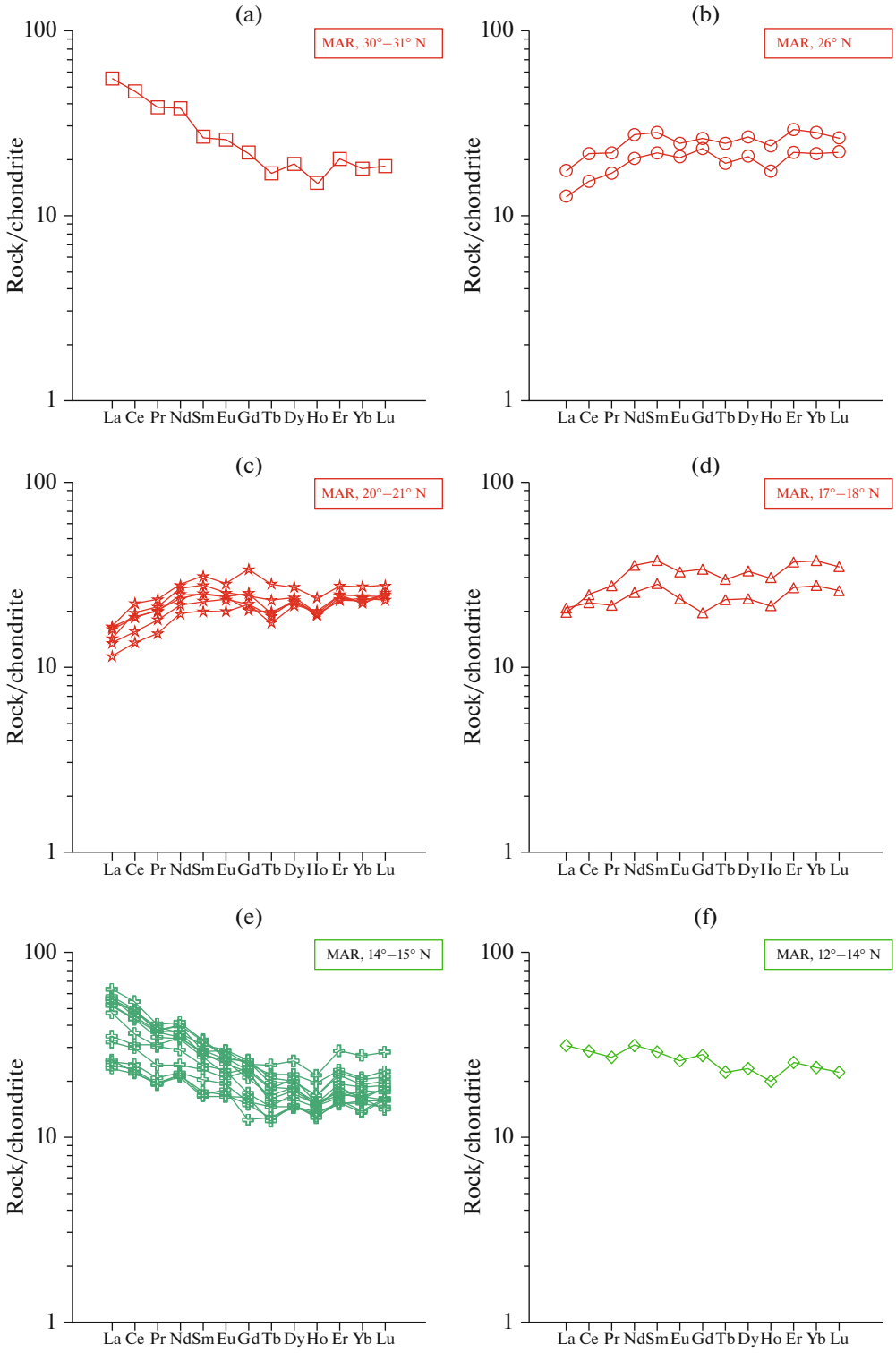

Fig. 3. Chondrite-normalized REE distribution patterns (determined by SIMS) in the studied chilled glasses of MORB: (a) MAR segment at 30°–31° N, (b) MAR segment at 26° N, (c) MAR segment at 20°–21° N, (d) MAR segment at 17°–18° N, (e) MAR segment at 14°–15° N, (f) MAR segment at 12°–14° N. Chondrite composition is taken from (Sun and McDonough, 1989). For symbols, see Fig. 2.

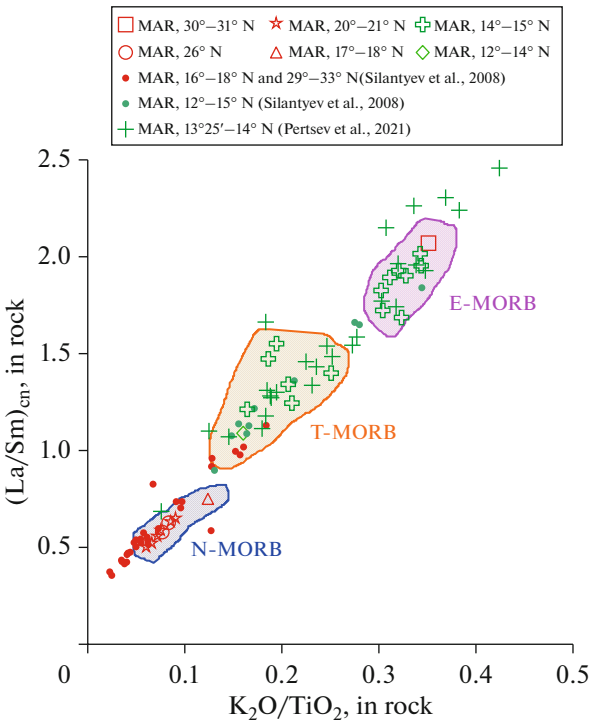

Fig. 4. Variations of K_2O/TiO_2 and $(La/Sm)_{cn}$ in the studied chilled glasses. Data points outlined by blue contour correspond to N-MORB; those, outlined by orange contour, to T-MORB; those outlined by violet contour, to E-MORB. Green crosses show variations of chilled glasses from the MAR axial zone within 13°25′–14° N presented in (Pertsev et al., 2021). Filled circles mean chilled glasses from the axial ridge zone between 12° and 34° N after (Silantyev et al., 2008): green data points show samples taken in the "cold" segments; red data points, in "hot" segments.

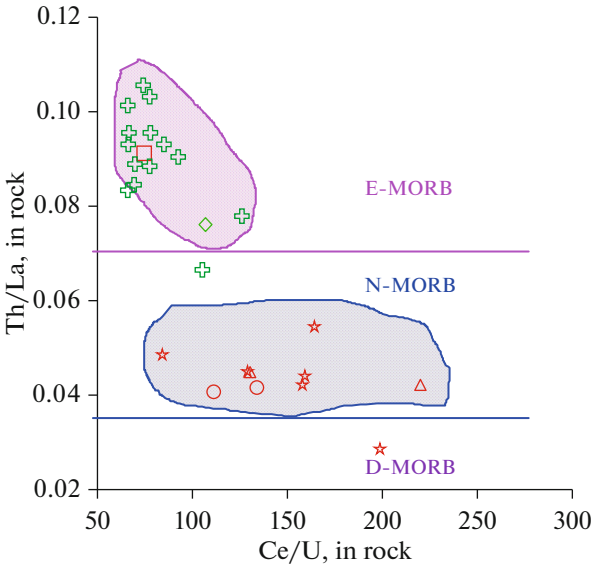

Fig. 5. Variations of Ce/U and Th/La in the studied chilled glasses (determined by SIMS). Fields of Th/La values typical of E-MORB, N-MORB, and D-MORB are shown after (Shimizu et al., 2016). For symbols, see Fig. 4.

melts. This is also confirmed by the covariations between Sr and MgO contents (Fig. 6b).

In chilled glasses of the E-MORB group, an increase of Sr contents at its much higher contents (≥200 ppm) also occurs within a sufficiently narrow range of K_2O/TiO_2 ratios, which significantly exceeds this parameter for N-MORB glasses. In general, data on the Sr content in the studied chilled glasses presented in Table 4 correspond to estimated contents of this element in different geochemical MORB types (e.g., Su, 2002; Arevalo and McDonough, 2010).

The scanning electron microscopic study of mineralogical features of the chilled glasses revealed no signs of their low-temperature alteration. However, some authors reported data on the contamination of parental MORB melts by volatile seawater or atmospheric components in magma chamber (Buikin et al., 2022) or when erupted magmas were quenched on seafloor (Broadley et al., 2017). The possible influence of such contamination on the composition of chilled glasses from the considered MAR segments was estimated using Cl and U contents (Table 4), which are the most mobile elements during interaction of oceanic crust with seawater and its hydrothermal derivatives (Verma, 1992; Clog et al., 2013). The absence of correlation between Cl and U contents and Sr concentrations in samples from basalt-dominated MAR segments may indicates that the Cl and U contents in N-MORB glasses show no significant variations and do not depend on the fractionation of parental melt (Fig. 8a—Cl and Fig. 8b—U). The consideration of Cl, U, and MgO covariations in chilled glasses collected in the basaltic segments of MAR allowed us also to conclude that Cl does not fractionate in the studied samples during the evolution of parental melt and its concentration remains at the level typical of depleted MORB (e.g., Michael and Cornell, 1998) (Fig. 9a). Uranium in glass samples taken from basaltic segments of MAR behave similarly to Cl (Fig. 9b) and reveals a narrow concentration range within limits typical of N-MORM and indicated, in particular, in (Arevalo and McDonough, 2010).

In contrast, the chilled glasses from MAR segments consisting mainly of serpentinites show the wide variations of Cl and U contents and their positive correlation with Sr concentration. Since U and Sr sharply differ in the mineral/melt partition coefficient (Sun et al., 2017), trend observed in Fig. 8b for glasses from these MAR segments was not caused by fractionation crystallization and likely reflects the contamination of melt by hydrothermal fluid—seawater derivative. Data points of E-MORB chilled glasses taken from serpentinite segments of MAR occupy much wider field in Fig. 9 compared to N-MORB chilled glasses, and have much higher Cl and U contents. A positive cor-

Table 4. Content of some trace elements in the studied chilled glasses.

Sample no.	Ba	Th	U	Nb	Ta	Pb	Sr	Zr	Hf	Y	Cl*	B	Li	Be
16ABP7-8	139.89	1.19	0.39	20.41	1.40	1.32	224	118	4.59	24.77	250	0.99	4.277	0.76
64gl	14.44	0.17	0.12	3.43	0.83	0.91	131	112	4.99	38.09	50	1.11	5.188	0.56
14-3/1gl	11.04	0.13	0.07	2.85	0.65	0.74	124	80	3.79	30.48	60	0.79	4.669	0.46
36L12D-3	15.76	0.17	0.09	3.01	0.73	0.48	148	90	4.12	32.33	40	0.86	4.763	0.52
36L16D-3	9.14	0.11	0.05	2.13	0.68	0.44	97	67	3.71	31.21	40	0.57	4.102	0.32
36L29D-4	15.66	0.21	0.07	3.71	0.72	0.47	123	89	4.20	31.76	50	0.79	4.561	0.47
36L40D-3	8.81	0.15	0.11	2.42	0.72	0.79	115	81	4.06	31.73	40	0.72	4.713	0.41
36L44D-3	13.03	0.17	0.08	3.04	0.87	0.75	144	114	5.12	37.21	30	0.93	5.405	0.53
36L46D-2	10.60	0.09	0.06	3.07	0.78	0.55	160	90	4.23	32.67	40	0.85	4.850	0.47
36L233D-1	33.50	0.22	0.10	5.60	0.86	0.63	142	95	4.72	34.53	80	0.78	4.977	0.50
36L235D-1	12.35	0.19	0.07	3.46	1.05	1.28	117	134	6.27	48.66	40	1.15	6.634	0.61
16ABP54gl	69.25	0.54	0.18	10.76	1.18	1.13	160	121	5.21	37.71	130	1.11	5.877	0.70
16ABP70-31	121.83	1.13	0.40	18.39	1.14	0.99	216	109	3.97	23.92	230	0.98	4.166	0.75
16ABP71-13	53.54	0.50	0.18	7.62	0.70	0.42	149	65	3.19	18.80	90	0.61	3.232	0.42
16ABP67-9	126.77	1.25	0.41	20.38	1.19	1.22	212	115	4.56	24.70	190	0.98	3.953	0.76
16ABP70-32	127.23	1.14	0.31	18.71	1.28	1.12	222	120	4.31	26.54	230	1.01	4.338	0.73
16ABP65-34	126.02	0.92	0.32	16.66	1.25	1.13	197	92	3.33	22.93	220	0.83	3.893	0.60
16ABP69-13	54.39	0.47	0.11	7.82	0.70	0.58	148	64	2.99	20.61	110	0.63	3.292	0.42
16ABP69-11	55.38	0.57	0.19	8.08	0.75	0.59	155	66	2.70	20.28	100	0.64	3.397	0.43
16ABP69-10	52.37	0.51	0.16	7.82	0.60	0.46	148	61	2.71	19.58	100	0.61	3.319	0.40
16ABP70-34	116.86	1.07	0.38	18.13	1.11	1.03	207	109	3.96	23.62	240	0.98	4.185	0.71
16ABP67-7	81.47	0.80	0.25	11.06	0.81	0.59	167	83	3.24	21.61	150	0.81	4.112	0.53
2PD 44-1	152.07	1.12	0.45	21.70	1.38	0.91	238	117	4.48	26.30	210	0.90	4.242	0.75
2PD44-3	170.51	1.49	0.49	25.05	1.49	1.25	255	127	5.06	28.50	310	0.99	5.099	0.84
2PD45	139.19	1.34	0.37	20.77	1.32	1.19	218	122	4.79	26.13	290	0.99	4.512	0.77
2PD43-3	61.55	0.56	0.17	10.40	0.91	0.87	161	109	4.62	31.79	150	1.05	5.530	0.62

Contents of elements are given in ppm. * Microprobe data (EPMA).

relation between Cl and U contents (Fig. 10) as U–Sr trend typical of the same samples in Fig. 8b likely reflects the contamination of parental MORB melts by seawater components.

NATURE OF GEOCHEMICAL EVOLUTION TRENDS OF CHILLED GLASSES OF MAR

Consideration of presented above data in the light of the existing data on structure and composition of lithosphere of the MAR axial zone between 12° and 31° N indicates that practically all chilled glasses ascribed to E-MORB were taken from the "cold" MAR segments, with mainly serpentinite crust section (Fig. 11). At the same time, the N-MORB-type glasses from the studied collection were taken mainly in "hot" mainly basaltic segments of MAR. It should be emphasized that all presently known geochemical MORB types tightly associate in MAR in some areas of the MAR axial zone. This phenomenon reflects the fundamental feature of MAR, which is expressed in two types of its geochemical segmentation: large- and small scaled. The first type reflects thermal and, respectively, rheological state of mantle protolith generating parental melts of MORB. The small-scaled segmentation is formed by intracrustal processes related to the interaction of magmatic and hydrothermal systems in the MAR axial zone. These processes likely provided geochemical characteristics that are observed in MAR basalts and in many works are interpreted as obtained through recycling (e.g., Hemond et al., 2006).

During serpentinization, the ultramafic protolith of oceanic crust assimilates significant amounts of Cl, Sr, and U from seawater-derived fluid (Silantyev, 2003; Sharp and Barnes, 2004). The Sr and U variations in seprentinites associated with chilled glasses extracted between 12° and 15° N are seen in Fig. 12. The trends of Cl and U contents in enriched chilled glasses shown in Figs. 8–10 likely reflect the compositional peculiarity of associated serpentinites, which

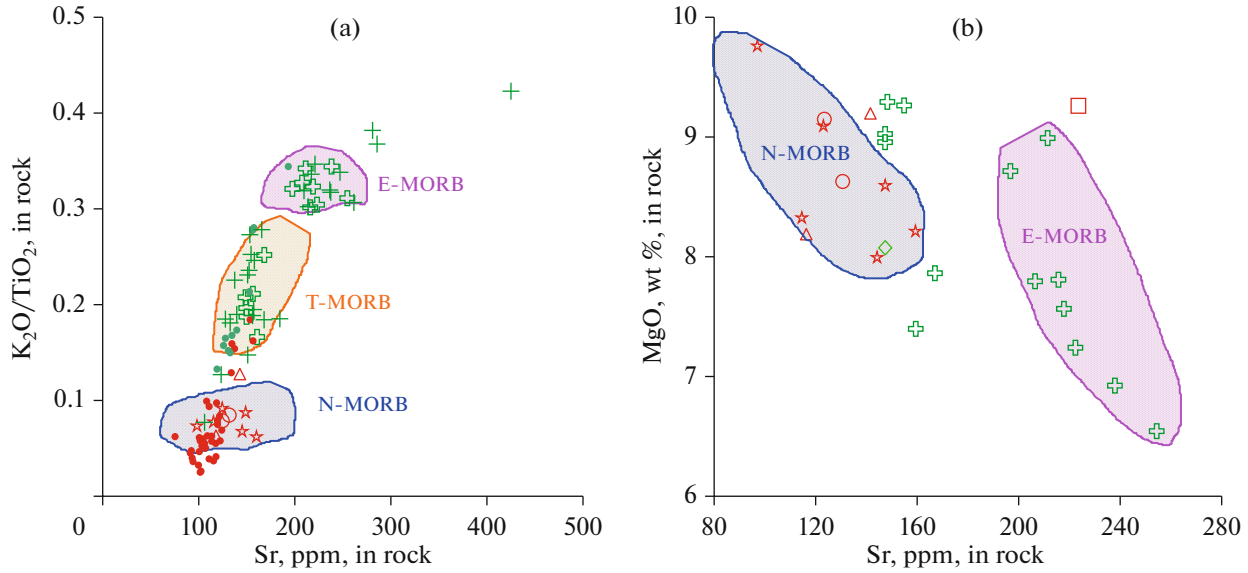

Fig. 6. Variations of Sr and K_2O/TiO_2 (a) and Sr and MgO (b) in the studied chilled glasses of MORB. For symbols, see Fig. 4.

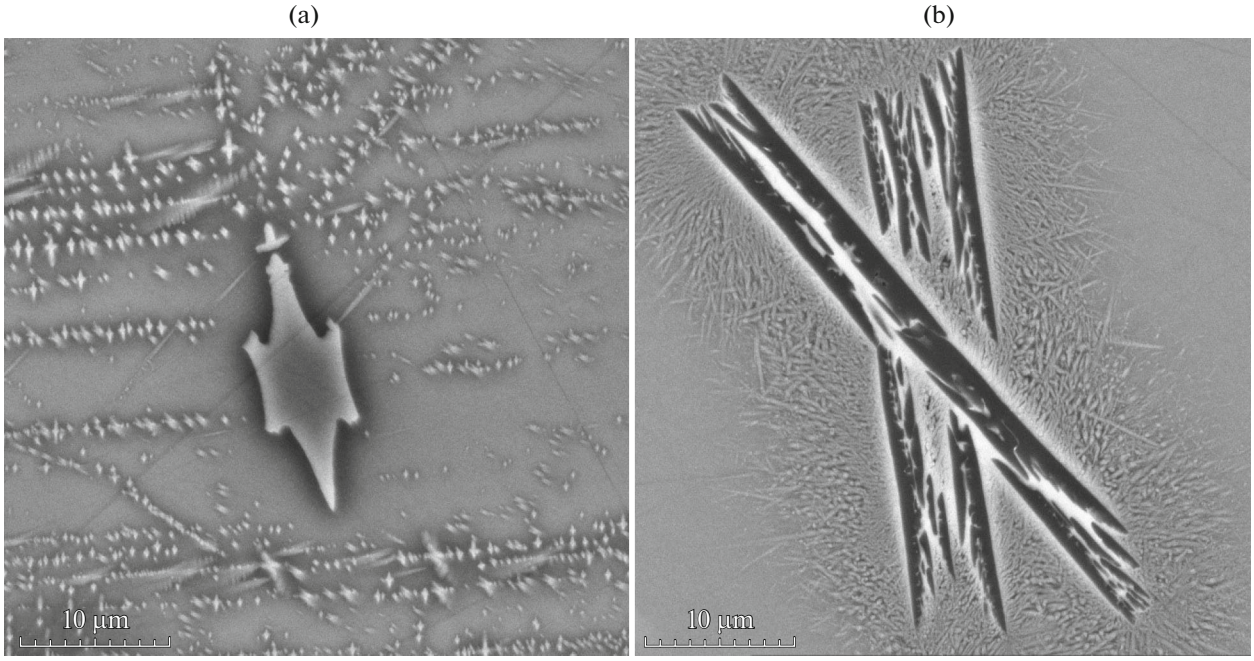

Fig. 7. Crystallites of olivine (a) and plagioclase (b) in chilled N-MORB glasses (samples 36L235D-1 and 14-3/1gl, correspondingly). The images were obtained using scanning electron microscope.

are the predominant rock type in these segments, while the products of basaltic magmatism in these segments are extremely scarce. Evidence for in situ contribution of hydrothermal component in the evolution of parental magmatic melt of MORB of the MAR rift valley were previously reported in (Kendrick et al., 2012; Stroncik and Niedermann, 2016; Buikin et al., 2022). Figure 13 demonstrates the Cl distribution in the MORB chilled glasses from MAR segments enclosed between 10° and 40° N. The chilled glasses with high Cl content are confined to the axial ridge zones that are made up of serpentinites and comprise so-called "serpentinite-hosted" hydrothermal fields. In contrast to the E-MORB glasses, samples of depleted chilled glasses (N-MORB), as follows from Figs. 11 and 13, are located in the basaltic segments of

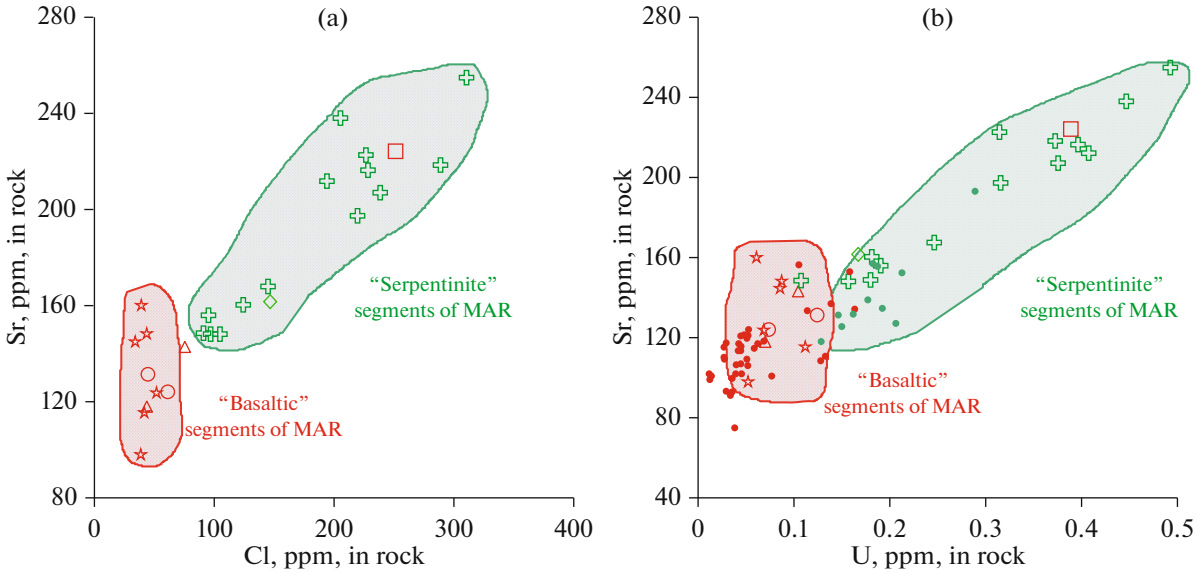

Fig. 8. Correlations of Cl (determined by EPMA) and Sr (a), as well as U and Sr (determined by SIMS) (b) in the studied MORB chilled glasses. For symbols, see Fig. 4.

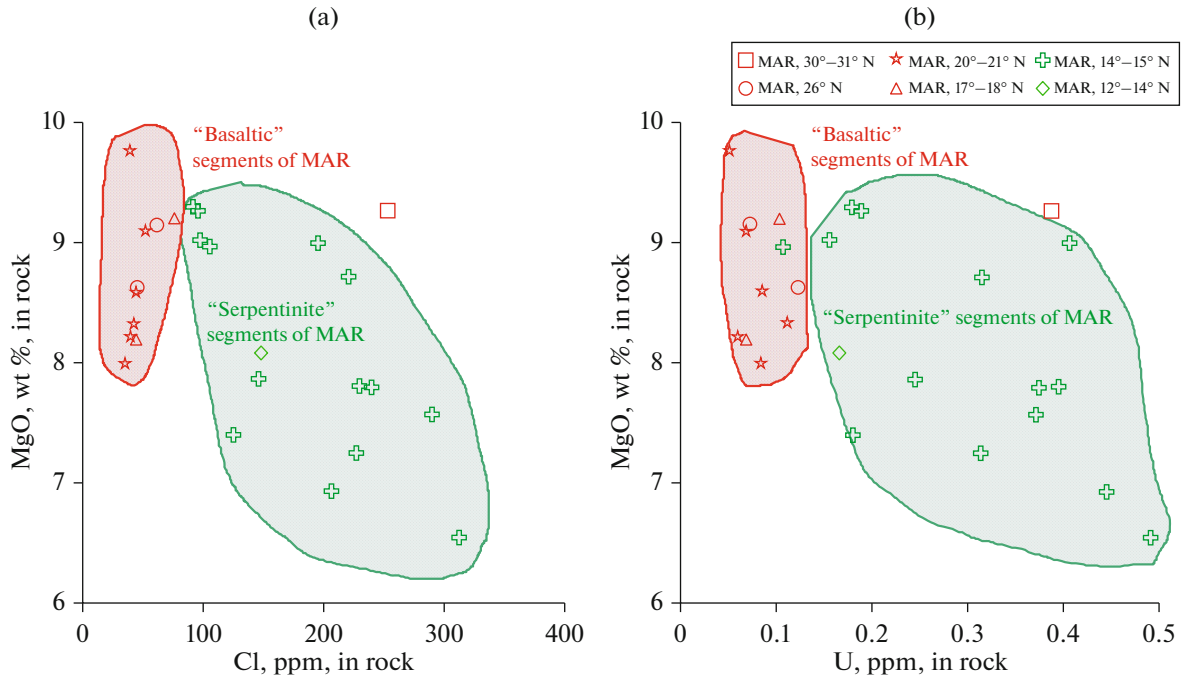

Fig. 9. Correlations of Cl and MgO (a) and U and MgO (b) in the studied chilled glasses of MORB.

the MAR axial zone, which enclose hydrothermal fields associated with basalts ("basalt hosted"). Judging from the above mentioned data, the signs of intracrustal contamination in glasses of this group are absent.

In spite of the fact that geochemical features of chilled glass presented by sample 16ABP7-8 indicate its unambiguous affiliation to E-MORB family, this sample was dredged from the axial volcanic uplift in the rift valley, while serpentinite exposures were not found in this area.

As seen in Figs. 11 and 13, the dredging station that yielded this sample is located 60 miles to the north of the large Broken Spur hydrothermal field. This field records the geochemical signs of active interaction of high-temperature hydrothermal fluid with basalts of

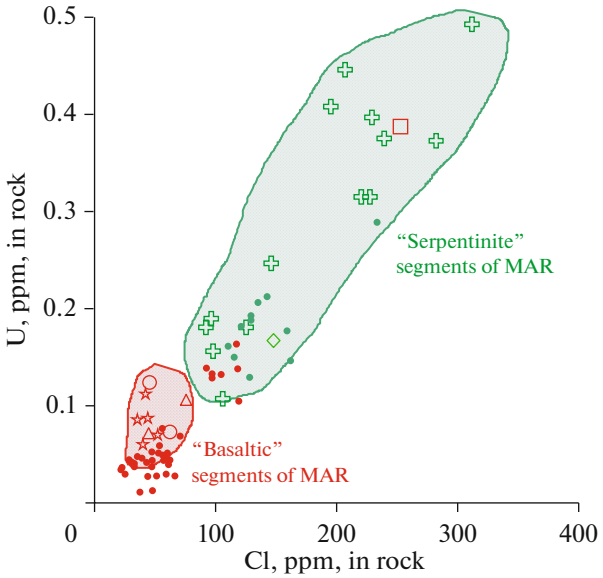

Fig. 10. Variations of Cl and U in the studied chilled glasses of MORB. For symbols, see Fig. 4.

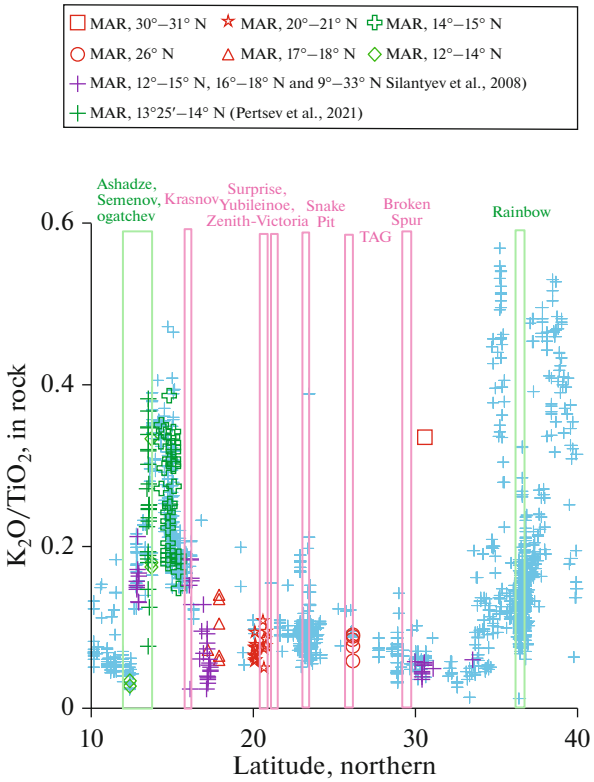

Fig. 11. Distribution of K_2O/TiO_2 ratio in chilled glasses of MORB along MAR axis between 10° and 40° N. Blue crosses are compositions taken from (*RIDGE* ..., 1999). Red color and its tints show the MAR axial zone areas, which comprise hydrothermal fields related to the basaltic protolith and data points of the studied chilled glasses dredged from these areas. Green color shows the areas of hydrothermal fields associated with serpentinites and compositions of studied chilled glasses from these areas. Thin green crosses are the compositions of chilled glasses from (Pertsev et al., 2021). Violet crosses show the compositions of chilled glasses from (Silantyev et al., 2008).

the rift valley (James et al., 1995). It is probable that the active hydrothermal circulation is traced also to the north of this field. The high Cl and U contents in this chilled glass is likely caused by the contamination of its parental melt by seawater-derived hydrothermal fluid. Previously, such mechanism of contamination was proposed to interpret data on H_2O and Cl contents, as well as He–Ar–N–C(CO_2) isotopic composition and element ratios in chilled glasses from the axial MAR zone at 16°09′ N, in the vicinity of the Krasnov hydrothermal field (Buikin et al., 2022). It is hardly probable that the high Cl content in the chilled glasses reflects the geochemical specifics of parental melts of E-MORB. Urann et al. (2017) reported arguments in support of opinion that the existing estimates of Cl content in the DMM reservoir are overestimated and require revision, whereas Cl content in MORB is almost always related to some MORB contamination by seawater or its derivatives.

It was noted above that chilled glasses of E-MORB family are restricted to the "cold" segments of MAR, which are dominated by serpentinites. This tendency provides a new insight into the problem of E-MORB origin in some MAR areas. At present, numerous finds of ancient zircons in magmatic products from the MAR crest zone allowed some researchers to suggest the contribution of relics of ancient continental lithosphere, which were preserved beneath axial zone of the ridge and were involved in partial melting of shallow mantle (Bortnikov et al., 2022). Some geochemical and petrological evidence also indicate that the considered segments of the MAR rift valley contain exotic lithospheric blocks: at 35°04′–35°30′ N (Dosso et al., 1999), 15°30′ N (Silantyev, 1998), and 10°42′ N (Kostitsyn et al., 2018). The presence of such relics of ancient lithosphere beneath some areas of the MAR axial zone is likely expressed in the alternation of its "cold" ("serpentinite") and "hot" ("basaltic") segments. We suggest that that the contribution of relics of ancient continental lithosphere in the magmatism of the MAR rift valley was responsible for the geochemical parameters of E-MORB group. This likely indicates that the rheological conditions favorable for the formation of long-lived magma chambers within oceanic crust are implemented in the "cold" MAR segments. Such style of magmatism in the low-velocity spreading center as MAR facilitates the contamination of basaltic melts by components assimilated from host serpentinites or from aqueous–saline fluids circulating in the "serpentinite hosted" hydrothermal systems.

The proposed model can be considered alternative to the concepts that the E-MORB origination in MAR segments between 14°–15° N and at 30° N was related

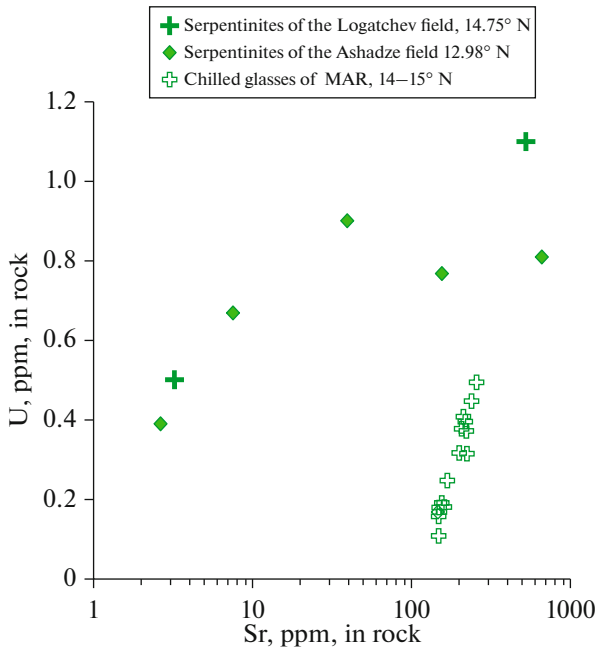

Fig. 12. Variations of U and Sr contents in the studied chilled glasses of MORB and associated serpentinites from MAR segments enclosed between 12° and 15° N. The composition of serpentinites was taken from (Silantyev et al., 2011).

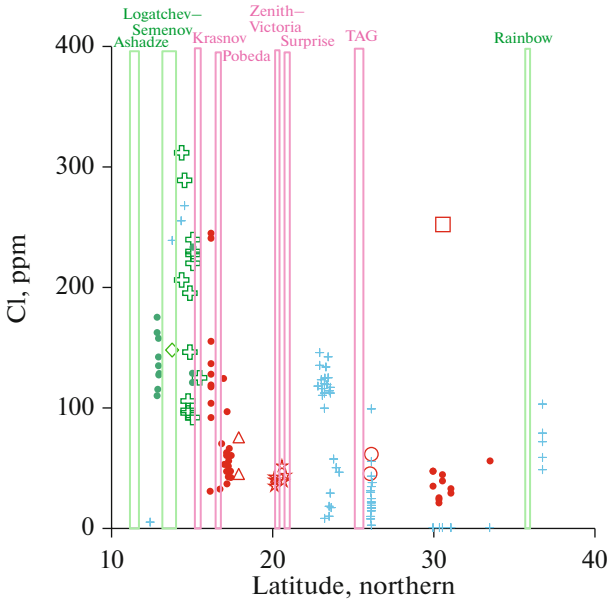

Fig. 13. Variations of Cl contents in MORB chilled glasses along MAR axis, between 10° and 40° N. For symbols, see Figs. 2 and 4.

to recycling of alkaline OIB-type basalts (e.g., Hemond et al., 2006). Yang et al. (2018) attempted to analyze the distribution of more than 60 elements in 319 samples of chilled glasses of D-MORB, N-MORB, and E-MORB from 144 separate lava flows in the MAR rift valley segments between 10° and 40° N. Results presented in this work demonstrated that the trace element ratios that are "sensitive" to fluid transport in subduction zone (Th/U, Nb/U, Ba/Th, Ba/La) are characterized by steady values that are similar to their mantle values for N- and E-MORB. Thus, obtained data (Yang et al., 2018) highlight the need in revision of genetic models explaining the enrichment of parental melts of MORB through recycling.

CONCLUSIONS

Presented data on the geochemical features of samples of chilled glasses taken from different MAR segments between 12° and 31° N allowed us to draw several conclusions that are of great importance not only for the assessment of possible influence of active hydrothermal systems on the geochemical parameters of MORB, but also for reconstructing the nature of sources of parental melts of E-MORB.

1. Basalts of E-MORB family, which includes the majority of chilled glass samples studied in this work, are localized mainly in "cold" segments of MAR, the crust section of which consists mainly of serpentinites.

2. Samples of depleted N-MORB chilled glasses are confined to segments of the MAR axial zone, in which serpentinites are either absent or occur in subordinate amount.

3. In chilled E-MORB glasses from "cold" MAR segments reveal signs of contamination of basaltic melts by components assimilated either from host serpentinites or from aqueous–saline fluids circulating in "serpentinite hosted" hydrothermal systems.

4. Obtained data on the distribution of Cl, U, and Sr in the studied chilled glasses ascribed to the N-MORB family show no signs of intracrustal contamination.

5. It is possible that relics of ancient continental lithosphere preserved beneath the axial ridge zones were involved in partial melting of shallow mantle and generation of parental melts of E-MORB in some MAR segments.

In future works dedicated to the discussed problem, we plan to analyze the isotopic compositions of Sr and Nd, as well as noble gases and nitrogen in the studied chilled glasses in order to confirm or revise presented above conclusions.

ACKNOWLEDGMENTS

We are grateful to N.M. Sushchevskaya for the provided samples of chilled glasses from MAR segment at 26° N. D.D. Badyukov is thanked for help with studies on a TESCAN MIRA3 electron microscope.

FUNDING

The study was supported by the Russian Science Foundation (project no. 22-27-00815).

CONFLICT OF INTEREST

The authors declare that they have no conflicts of interest.

REFERENCES

Andreani, M., Escartin, J., Delacour, A., et al., Tectonic structure, lithology, and hydrothermal signature of the Rainbow Massif (Mid-Atlantic Ridge 36°14′ N), *Geochem. Geophys. Geosyst,* 2014, vol. 15, pp. 3543–3571.

Arevalo, R.Jr. and McDonough, W.F., Chemical variations and regional diversity observed in morb, *Chem. Geol.,* 2010, vol. 271, pp. 70–85.

Becker, T.W. and Boschi, L., A comparison of tomographic and geodynamic mantle models, *Geochem. Geophys. Geosyst,* 2002, vol. 3, pp. 1–48.

Bel'tenev, V., Shagin, A., Markov, V., et al., A new hydrothermal field at 16° 38.4′ N, 46° 28.5′ W on the Mid-Atlantic Ridge, *InterRidge News,* 2004, no. 13, pp. 5–6.

Bel'tenev, V.E., Rozhdestvenskaya, I.I., Samsonov, I.K., et al., Prospecting Works on the Area of the Russian Project Area in the Atlantic Ocean with Appraisal of inferred resources GPS of categories R2 and R3 in Blocks 31–45 (Lomonosov: Fondy FGUNPP "PMGRE", 2016).

Bel'tenev, V.E., Lazareva, L.I., Cherkashev, G.A., et al., New hydrothermal sulfide fields of the Mid-Atlantic Ridge: Yubileinoe (20°09′ N) and Surprise (20°45.4′ N), *Dokl. Earth Sci.,* 2017, vol. 476, no. 3, pp. 1010–1015.

Bogdanov, Yu.A., Lisitsyn, A.P., Sagalevich A.M., and Gurevich, E.G., *Gidrotermal'nyi rudogenez okeanskogo dna* (Hydrothermal Ore Genesis of Ocean Floor), Moscow: Nauka, 2006.

Bonatti, E., Peyve, A., Kepezhinskas, P., et al., Upper mantle heterogeneity below Mid-Atlantic Ridge 0°–15° N, *J. Geophys. Res.,* 1992, vol. 97.

Bortnikov, N.S., Silantyev, S.A., Bea, F., et al., Multiple melting of a heterogeneous mantle and episodic accretion of oceanic crust in a spreading zone: zircon U-Pb age and Hf-O isotope evidence from an oceanic core complex of the Mid-Atlantic Ridge, *Petrology,* 2022, vol. 30, no. 1, pp. 1–24.

Bottazzi, P., Ottolini, L., Vannucci, R., and Zanetti, A., *An accurate procedure for the quantification of rare earth elements in silicates, IMS IX Proceedings,* Benninghoven, A., Nihei, Y., Shimizu, R., and Werner, H.W., Eds., Chichester: Wileys, 1994, pp. 927–930.

Bougault, H., Dmitriev, L., Schilling, J.-G., et al., Mantle heterogeneity from trace elements: MAR triple junction near 14° N, *Earth Planet. Sci. Lett.,* 1988, vol. 88, pp. 27–36.

Broadley, M.W., Burgess, R., Kumagai, H., et al., Halogen variations through the quenched margin of a morb lava: evidence for direct assimilation of seawater during eruption, *Geochem. Geophys. Geosyst.,* 2017, vol. 18, pp. 2413–2428.

Buikin, A.I., Silantyev, S.A., and Verchovsky, A.B., N-Ar-He-CO_2 systematics combined with H_2O, Cl, K abundances in MORB glasses demonstrate interaction of magmatic and hydrothermal systems: a case for MAR at 16°07′-17°11′ N, *Geochem Int.,* 2022, vol. 60, no. 11, pp. 1068–1086.

Cannat, M. and Casey, J.F., *An ultramafic lift at the Mid-Atlantic Ridge: successive stages of magmatism in serpentinized peridotites from the 15° N region, Mantle and Lower Crust Exposed in Oceanic Ridges and in Ophiolites*, Vissers, R.L.M. and Nicolas, A., Eds., Kluwer Academic Publ., 1995, pp. 5–34.

Casey, J.F., Comparison of major and trace-element geochemistry of abyssal peridotites and mafic plutonic rocks with basalts from the Mark region of the Mid-Atlantic Ridge, Karson, J.A., Cannat, M., Miller, D.J., and Elthon, D., Eds., *Proceedings of the Ocean Drilling Program, Sci. Res,* 1997, vol. 153, pp. 181–241.

Cherkashov, G., Poroshina, I., Stepanova, T., et al., Seafloor massive sulfides from the northern equatorial Mid-Atlantic Ridge: new discoveries and perspectives, *Mar. Geores. Geotechnol.,* 2010, vol. 28, no. 3, pp. 222– 239.

Clog, M., Aubaud, C., Cartigny, P., and Dosso, L., The hydrogen isotopic composition and water content of southern Pacific MORB: a reassessment of the D/H ratio of the depleted mantle reservoir, *Earth Planet. Sci. Lett.,* 2013, vol. 381, pp. 156–165.

Dick, H.J.B., Lissenberg, C.J., and Warren, J.M., Mantle melting, melt transport, and delivery beneath a slow-spreading ridge: the paleo-mar from 23°15′ N to 23°45′ N, *J. Petrol.,* 2010, vol. 51, nos. 1–2, pp. 425–467.

Dmitriev, L.V., Chemical variability of mid-ocean ridge basalts as a function of the geodynamic setting of their formation, *Petrology,* 1998, vol. 6, no. 4, pp. 314–334.

Dmitriev, L.V. and Sokolov, S.Yu., Geodynamics of three contrasting types of oceanic magmatism and their reflection in the data of seismic tomography, *Petrology,* 2003, vol. 11, no. 6, pp. 597–613.

Dmitriev, L.V., Sokolov, S.Yu., and Plechova, A.A., Statistical assessment of variations in the compositional and P–T parameters of the evolution of mid-oceanic ridge basalts and their regional distribution, *Petrology,* 2006, vol. 14, no. 2, pp. 209–229.

Dosso, L., Hanan, B.B., Bougault, H., et al., Sr–Nd–Pb geochemical morphology between 10° and 17° N on the Mid-Atlantic Ridge: a new MORB isotope signature, *Earth Planet. Sci. Lett.,* 1991, vol. 106, pp. 29–43.

Dosso, L., Bougault, H., Langmuir, C., et al., The age and distribution of mantle heterogeneity along the Mid-Atlantic Ridge (31°–41° N), *Earth Planet. Sci. Lett.,* 1999, vol. 179, pp. 269–286.

Eason, D. and Sinton, J., Origin of high-Al N-MORB by fractional crystallization in the upper mantle beneath the Galapagos spreading center, *Earth Planet. Sci. Lett.,* 2006, vol. 252, pp. 423–436.

Fedotova, A.A., Bibikova, E.V., and Simakin, S.G., Ion-microprobe zircon geochemistry as an indicator of mineral genesis during geochronological studies, *Geochem. Int.,* 2008, vol. 46, no. 9, pp. 912–927.

Firstova, A., Stepanova, T., Cherkashev, et al., Composition and formation of gabbro-peridotite hosted seafloor massive sulfide deposits from the Ashadze-1 hydrothermal field, Mid-Atlantic Ridge, *Minerals,* 2016, vol. 6, no. 19. https://doi.org/10.3390/min6010019

Grand, S.P., van der Hilst, R.D., and Widiyantoro, S., Global seismic tomography: a snapshot of convection in the earth, *GSA Today,* 1997, vol. 7, no. 4, pp. 1–7.

Grand, S.P., Mantle shear-wave tomography and the fate of subducted slabs, *Phil. Trans. R. Soc. London,* 2002, vol. 360, pp. 2475–2491.

Halliday, A.N., Lee, D.-C., Tommasini, S., et al., Incompatible trace elements in OIB and MORB and source enrichment in the sub-oceanic mantle, *Earth Planet. Sci. Lett.,* 1995, vol. 133, pp. 379–395.

Hemond, C., Hofmann, A.W., Vlastelic, I., and Nauret, F., Origin of MORB enrichment and relative trace element compatibilities along the Mid-Atlantic Ridge between 10° and 24° N, *Geochem. Geophys. Geosyst.,* 2006, vol. 7, no. 12, Q12010,
https://doi.org/10.1029/2006GC001317

Humphris, S.E., Tivey, M.K., and Tivey, M.A., The trans-Atlantic geotraverse hydrothermal field: a hydrothermal system on an active detachment fault, *Deep Sea Research Part II: Topical Studies in Oceanography,* 2015, vol. 121, pp. 8–16.

James, R.H., Elderfield, H., and Palmer, M.R., The chemistry of hydrothermal fluids from the Broken Spur site, 29° N Mid-Atlantic Ridge, *Geochim. Cosmochim. Acta,* 1995, vol. 59, no. 4, pp. 651–659.

Jochum, K.P., Dingwell, D.B., Rocholl, A., et al., The preparation and preliminary characterisation of eight geological MPI-DING reference glasses for in situ microanalysis, *Geostand. Newslett.,* 2000, vol. 24, pp. 87–133.

Kendrick, M.A., Kamenetsky, V.S., Phillips, D., and Honda, M., Halogen systematics (Cl, Br, I) in mid-ocean ridge basalts: a Macquarie Island case study, *Geochim. Cosmochim. Acta,* 2012, vol. 81, pp. 82–93.

Klein, E.M. and Langmuir, C.H., Global correlations of ocean ridge basalt chemistry with axial depth and crustal thickness, *J. Geophys. Res.,* 1987, vol. 92, pp. 8089–8115.

Klitgord, K.D., Dmitriev, L.V., Casey, J.F., et al., 12th Cruise of the R/V *Akademik Boris Petrov*, (leg 1)/February 2-February 28, 1989. U.S. Soviet Collaborative Geological And Geophysical Survey of the Mid-Atlantic Ridge near 31° N. The Petrov Fracture Zone, *U.S. Geol. Survey Open File Report,* nos. 94-7, (1993).

Kostitsyn, Yu.A., Silantyev, S.A., Anosova, M.O., et al., Age of plutonic rocks from the Vema Fracture Zone (Central Atlantic) and nature of their mantle sources, *Geochem. Int.,* 2018, vol. 56, no. 2, pp. 89–110.

Maslennikov, V.V., Cherkashov, G.A., Artemyev, D.A., et al., Pyrite varieties at Pobeda hydrothermal fields, Mid-Atlantic Ridge 17°07′–17°08′ N: LA-ICP-MS data deciphering, *Minerals,* 2020, vol. 10, no. 7.
https://doi.org/10.3390/min10070622

Melekestseva, I., Maslennikov, V.V., Safina, N.P., et al., Sulfide breccias from the Semenov-3 hydrothermal field, Mid-Atlantic Ridge: authigenic mineral formation and trace element pattern, *Minerals,* 2018, vol. 8, no. 321.
https://doi.org/10.3390/min8080321

Michael, P.J. and Cornell, W.C., Influence of spreading rate and magma supply on crystallization and assimilation beneath mid-ocean ridges: evidence from chlorine and major element chemistry of mid-ocean ridge basalt, *J. Geophys. Res.,* 1998, vol. 103.

Murton, B.J., Van Dover, C., and Southward, E., Geological setting and ecology of the Broken Spur hydrothermal vent field: 29°10′ N on the Mid-Atlantic Ridge, *Geol. Soc. London: Spec. Publ.*, 1995, vol. 87, pp. 33–41.

Nosova, A.A., Sazonova, L.V., Narkisova, V.V., and Simakin, S.G., Minor elements in clinopyroxene from Paleozoic volcanics of the Tagil Island Arc in the Central Urals, *Geochem. Int.,* 2002, vol. 40, no. 3, pp. 219–232.

Pertsev, A.N., Aranovich, L.Ya., Prokofiev, V.Y., et al., Potassium-rich granite melt inclusions in zircon from gabbro-hosted felsic stringers, Mid-Atlantic Ridge at 13°34′ N: E-MORB connection, *Lithos,* 2021, vol. 400–401, p. 106300.

RIDGE Petrological Data Base, LGEO, 1999.

Rona, P.A., Tag hydrothermal field: Mid-Atlantic Ridge crest at latitude 26° N, *J. Geol. Soc.,* 1980, vol. 137, pp. 385–402.

Rona, P.A., Hannington, M.D., Raman, C.V., et al., Active and relict sea-floor hydrothermal mineralization at the TAG hydrothermal field. Mid-Atlantic Ridge, *Econ. Geol.,* 1993, vol. 88, pp. 1989–2017.

Sarda, P. and Graham, D., Mid-ocean ridge popping rocks: implications for degassing at ridge crests, *Earth Planet. Sci. Lett.,* 1990, vol. 97, pp. 268–289.

Schilling, J.-G., Zajac, M., Evans, R., et al., Petrologic and geochemical variations along the Mid-Atlantic Ridge from 27° and 73° N, *Am. J. Sci.,* 1983, vol. 283, pp. 510–586.

Shipboard Scientific Party. *Drilling Mantle Peridotite along the Mid-Atlantic Ridge from 14° to 16° N, Ocean Drilling Program, Leg 209 Preliminary Report,* Texas A&M University, College Station TX, 2003.

Shipboard Scientific Party. *SERPENTINE. Scientific Cruise Report.* Iferemer – Centre de Brest, 2007.

Sharp, Z.D. and Barnes, J.D., Water-soluble chlorides in massive seafloor serpentinites: a source of chloride in subduction zones, *Earth Planet. Sci. Lett.,* 2004, vol. 226, pp. 243–254.

Shimizu, K., Saal, A.E., Myers, C.E., et al., Two-component mantle melting-mixing model for the generation of mid-ocean ridge basalts: implications for the volatile content of the pacific upper mantle, *Geochim. Cosmochim. Acta,* 2016, vol. 176, pp. 44–80.

Silantyev, S.A., Origin conditions of the Mid-Atlantic Ridge plutonic complex at 13°–17° N, *Petrology,* 1998, vol. 6, no. 4, pp. 351–387.

Silantyev, S.A., Variations in the geochemical and isotopic characteristics of residual peridotites along the Mid-Atlantic Ridge as a function of the nature of the mantle magmatic sources, *Petrology,* 2003, vol. 11, no. 4, pp. 305–326.

Silantyev, S.A., Danyushevsky, L.V., Plechova, A.A., et al., Geochemical and isotopic signatures of magmatic products in the MAR rift valley at 12°49′–17°23′ N and 29°59′–33°41′ N: evidence of two contrasting sources of the parental melts, *Petrology,* 2008, vol. 16, no. 1, pp. 36–62.

Silantyev, S.A., Mironenko, M.V., and Novoselov, A.A., Hydrothermal systems in peridotites of slow-spreading mid-oceanic ridges. Modeling phase transitions and material balance: downwelling limb of a hydrothermal circulation cell, *Petrology,* 2009, vol. 17, no. 2, pp. 138–157.

Silantyev, S.A., Krasnova, E.A., Kannat, M., et al., Peridotite–gabbro–trondhjemite association of the Mid-Atlantic Ridge between 12°58′ and 14°45′ N: Ashadze and Lo-

gachev hydrothermal vent fields, *Geochem. Int.* 2011, vol. 49, no. 4, pp. 323–354.

Silantyev, S.A., Bortnikov, N.S., Shatagin, K.N., et al., Peridotite–basalt association at MAR between 1942' and 1959' N: evaluation of petrogenetic conditions and material balance during hydrothermal transformation of the oceanic crust, *Petrology,* 2015, vol. 23, no. 1, pp. 1–21.

Smirnov, V.K., Sobolev, A.V., Batanova, V.G., et al., Quantitative sims analysis of melt inclusions and host minerals for trace elements and H_2O, *EOS Trans. Spring Meet. Suppl. AGU,* 1995, vol. 17, p. 270.

Sokolov, S.Y., Chamov, N.P., Khutorskoy, M.D., and Silantyev, S.A., Intensity indicators of geodynamic processes along the Atlantic–Arctic rift system, *Geodynam. Tectonoph,* 2020, vol. 11, no. 2, pp. 302–319.

Stroncik, N.A. and Niedermann, S., Atmospheric contamination of the primary Ne and Ar signal in mid-ocean ridge basalts and its implications for ocean crust formation, *Geochim. Cosmochim. Acta,* 2016, vol. 172, pp. 306–321.

Su, Y.J., Mid-Ocean Ridge Basalt Trace Element Systematics: Constraints from Database Management, ICP-MS Analyses, Global Data Compilation, and Petrologic Modeling. *Ph.D. Thesis,* New York: Columbia University, 2002.

Sukhanova, A.A., Mineralogical-Geochemical Features of AbyssalSulfide Ores of the Yubileinoe Field (Russian Prospecting Area of the Mid-Atlantic Ridge), *Candidate's (Geol.-Min.) Dissertation,* St. Petersburg: Gosudarstvennyi gornyi un-t, 2018.

Sun, S.-S. and McDonough, W.F., *Chemical and isotopic systematics of oceanic basalts: implications for mantle composition and processes, Magmatism in Ocean Basins*, Saunders, A.D. and Norry, M.J., Eds., *Geol. Soc. Spec. Publ. London,* 1989, vol. 42, pp. 313–345.

Sun, C., Graff, M., and Liang, Y., Trace element partitioning between plagioclase and silicate melt: the importance of temperature and plagioclase composition, with implications for terrestrial and lunar magmatism, *Geochim. Cosmochim. Acta,* 2017, vol. 206, no. 3.
https://doi.org/10.1016/j.gca,2017.03.003

Urann, B.M., Le Roux, V., Hammond, K., et al. Fluorine and chlorine in mantle minerals and the halogen budget of the Earth's mantle, *Contrib. Mineral. Petrol.,* 2017.
https://doi.org/10.1007/s00410-017-1368-7

Verma, S.P., Seawater alteration effects on REE, K, Rb, Cs, Sr, U, Th, Pb and Sr-Nd-Pb isotope systematics of mid-ocean ridge basalt, *Geochem. J.,* 1992, vol. 26, pp. 159–177.

Wilson, M., *Igneous Petrogenesis,* London: Unwin Hyman, 1989.

Winter, J.D., *An Introduction to Igneous and Metamorphic Petrology,* New York: Prentice Hall, 2001.

Yang, S., Humayun, M., and Salters, V.J.M., Elemental systematics in MORB glasses from the Mid-Atlantic Ridge, *Geochem. Geophys. Geosyst,* 2018, vol. 19, pp. 4236–4259.

Translated by M. Bogina